The peptide sensor motifs asymmetrically couple ATP hydrolysis to transport in the heterodimeric ABC transporter TmrAB

Cinthia R. Millan[1], Martina Francis[1], Valery F. Thompson[1], Tarjani M. Thaker[1], Thomas M. Tomasiak[1]*

From the [1]Department of Chemistry and Biochemistry, University of Arizona, Tucson, AZ 85721

Running title: Asymmetric allosteric coupling by TmrAB peptide sensors

*To whom correspondence should be addressed: Thomas M. Tomasiak: Department of Chemistry and Biochemistry, University of Arizona, Tucson, AZ 85721; tomasiak@email.arizona.edu; Tel. (520) 621-4646

Keywords: ABC transporter, ATPase, transporter, peptide transport, conformational change

ABSTRACT

ATP binding cassette (ABC) transporters participate in many processes central to life including cell wall biosynthesis, lipid homeostasis, and drug efflux. Large conformational rearrangements accompany transport and allosterically couple substrate transport in the transmembrane region to dimerization of nucleotide binding domains (NBDs) nearly ~30-40Å away in the cytoplasm. How the two binding sites coordinate remains elusive, particularly in a class of ABC transporters with only one catalytically competent NBD, the asymmetric ABC transporters. The peptide transporter TmrAB from *Thermus thermophilus* is one such asymmetric transporter, and here we present biochemical evidence that substrate binding couples to ATP binding in nonequivalent ways through each half of the TmrAB heterodimer. Specifically, we show that this unique mechanism depends on a highly conserved electrostatic motif in a region previously termed the peptide sensor. In this conformationally dynamic region, we demonstrate that mutation of an absolutely conserved glycine in the catalytically active TmrA chain (G131A) accelerates ATPase activity while uncoupling substrate binding from ATP hydrolysis. Surprisingly, mutation of the conserved glycine in the non-functional TmrB chain (G116A) resulted in the opposite effect in which ATPase activity is decreased with little effect on substrate binding. Our findings highlight an intrinsic asymmetry extending beyond that of the NBDs in asymmetric ABC transporters and support a mechanism where the peptide sensor in each half of TmrAB plays different roles in substrate transport.

Introduction

ABC transporters move substrates vital to cellular homeostasis including lipids, drugs, toxins, and peptides (1–3) through the use of ATP. Substrate transport likely takes place in all transporters by the alternating access model in which interconversion of an inward-facing high-affinity state to an outward-facing low-affinity state drives net transport (4). These conformational changes occur in an architecture comprised of two transmembrane domains (TMDs) and two nucleotide binding domains (NBDs) connected by intracellular loops (ICL) that are helical extensions of the TMD (**Figure 1A**). The predominant model that explains these transitions specifically for ABC transporters remains the switch model where alternating access is driven by three coupled events: 1) ATP-induced NBD dimerization 2) inward-facing to outward-facing transitions of a substrate binding site in the TMD, and 3) ATP hydrolysis to reset the transport cycle (5). Recent findings offer modified versions of the switch model (6, 7). In one, ATP hydrolysis drives formation of the outward-facing state (6). In the second variation, ATP hydrolysis drives the release of substrate (7). Both models propose multiple additional intermediate states (many of which are asymmetric), however the general concept of two NBDs coming together to drive transition to the outward-facing state remains intact (6, 7). These transitions can often be readily identified biochemically as changes in the ATPase rate upon

substrate binding or in substrate affinity upon ATP binding.

The junction between the NBDs and the TMDs has been identified as one critical coupling area in ABC1 family ABC exporters, the largest family of exporters in the ABC superfamily that includes the medically important members MsbA, P-glycoprotein (Pgp), CFTR, and MRP-1(3). Particular emphasis has been placed on the specific loops that extend from the NBDs to bridge contacts between bound ATP and the TMD. These loops, termed the Q-loop and X-loop, have been identified as critical interdomain coupling sites in Pgp, BmrA, and transporter associated with antigen processing -1/2 (TAP1/TAP2) (2, 8, 9). The cytoplasmic intracellular loops 1 and 2 (ICL1 and ICL2) are TMD extensions also implicated as critical for allosteric coupling in ABC1 family exporters, but comparatively less focus has been placed on their investigation (2). Here, a "peptide sensor" in ICL1 between transmembrane helices 2 (TM2) and 3 (TM3) and consisting of a series of charged and polar residues was suggested as important for allosteric coupling of the NBD and TMD (1, 2). The peptide sensor sequence consists of a charged residue in every 4th position of the ICL1 helix, just below a "tetrahelix bundle" (10) also identified as an important charged element for transport in MsbA (11).

Catalytically symmetric exporters like TAP1/TAP2, as well as its bacterial homolog *Thermus thermophilus* multi-drug resistance proteins A and B (TmrAB), accomplish transport with only one NBD functional for ATP hydrolysis. The TmrA subunit contains a canonical Walker B motif (φφφφE – where φ is any hydrophobic residue) and is capable of ATP hydrolysis, whereas the TmrB half contains a degenerate Walker B motif (φφφφD) and is deficient in ATP hydrolysis due to a glutamate to aspartate substitution. TmrAB transports lipid (12), drug-like dyes, and peptide substrates (13, 14), and remarkably can functionally replace TAP1/TAP2 in human macrophages (14, 15). Such an asymmetric transporter offers an excellent simplified model system for understanding the coupling between ATP binding/hydrolysis and substrate transport. Structures of TmrAB (14, 16, 17) and of TAP1/TAP2 (18) have revealed similar architectures to each other as well as other homodimeric ABC transporters, suggesting insights into their activation mechanisms may be informative on the regulation of the protein superfamily as a whole.

Recently, a cryo-EM structure determination of several conformational cycle endpoints in TmrAB provided snapshots into ATP coupling with substrate transport (7), broadly reflecting isolated states observed in other ABC transporter structures (7, 19, 20). Many changes are found throughout the transporter structure. Notably, residues corresponding to the peptide sensor in TmrAB form a helix that undergoes large conformational changes between inward-facing and outward-facing states (**Figure 1B**). Several new hydrogen bond networks are formed in the outward-facing state of the catalytically competent TmrA chain (**Figure 1B**, left panels): D140 in the peptide sensor bridges interactions between R206 on TM4 and R136 of the peptide sensor, while R132 bonds with N128 of coupling helix 1 (CH1). A completely different set of interactions is formed in the outward-facing state of TmrB (**Figure 1B**, right panels): D125 in the equivalent position to D140 in TmrA bridges interactions between the TM6 residues S308 and R311, while D117 in the equivalent position to R132 in TmrA bridges interactions between R121 of the peptide sensor motif and D195 on TM4.

In this work we identified a great degree of consensus of the peptide sensor across ABC1 family ABC exporters by aligning over 200+ sequences per monomer (**Supplemental Figures 1, 2**). Our analysis follows up on previous characterization of the peptide sensor (1, 2) and specifically defines $G(R/D)x_3Rx_3D$ as the peptide sensor consensus sequence in which charged residues are highly conserved and the glycine residue is absolutely conserved (**Figure 1C**). In TmrAB, the charged residues form a conserved π-helix following a critical hinge formed by the absolutely conserved glycine (G131 in TmrA, G116 in TmrB). This motif is likely functionally significant given the high level of evolutionary sequence conservation, the conserved π-helix, and the dynamic rearrangement of interactions observed between the inward and outward-facing structures.

Do the conserved features of the peptide sensor contribute to allosteric regulation of transport and the transition from inward-facing to outward-facing in TmrAB? Furthermore, is the conformational asymmetry of the peptide sensor helix a reflection of the functional asymmetry in the TmrAB NBDs? Here we address these questions and investigate the importance of the peptide sensor helical motif in the TmrAB transport cycle. We developed several peptide sensor mutants and biochemically

investigated their role in the allosteric coupling of ATP binding and hydrolysis to substrate binding and transport. We show that these mutations disrupt the ATPase catalytic cycle in both chains of TmrAB. We also show that in TmrA, but not TmrB, the peptide sensor motif is critical in initiating a low-affinity outward-facing state, revealing a dramatic intrinsic asymmetry of the transport cycle in TmrAB. Our findings suggest that the peptide sensor has important implications on relaying information from the "active" NBD (TmrA) to the rest of the molecule.

Experimental procedures

Molecular biology and cloning – Mutants of TmrAB were generated from the TmrAB pet22b template described in Zutz et al (13). Primers for site-directed mutagenesis were designed against the target region using the technique described by Liu and Naismith (21). Constructs were amplified by PCR and verified by sequencing (Elim Biopharmaceuticals, Inc.).

Large scale sequence alignments – 250 sequences similar to TmrA (**Supplemental Figure 1**) and 250 sequences similar to TmrB (**Supplemental Figure 2**) of bacterial origin were downloaded from the UniProt database and aligned in MUSCLE 3.8 (22). After manual inspection for gaps and coverage of both domains, 48 sequences were omitted from TmrA alignment, and the rest subject to conservation analysis (**Figure 1C**).

Protein expression and purification –Wild-type (WT) and mutant TmrAB were expressed and purified using the method previously described by Zutz et al. (13). Briefly, a starter culture of BL21(DE3) *E. coli* (NEB) cells transformed with TmrAB were incubated for 16 hours overnight with shaking at 37°C in 10 mL of Luria Broth (LB) supplemented with ampicillin. On the following day, 1L of Terrific Broth (TB) media was inoculated with 5-10 mL of the overnight culture and cells grown at 37°C until an OD_{600} of ~0.8 was reached. TmrAB expression was induced with 1 mM IPTG and cells cultured at 37°C for an additional 4 hours prior to harvest at 4°C by centrifugation at 5000xg for 20 min. For the G131A mutation, cells were cultured at room temperature for an additional 16 hours following induction.

Protein was purified first by resuspending cell pellets in lysis buffer (50 mM Tris-HCl, 300 mM NaCl, pH 8.0, and protease inhibitor tablets (Roche)) and lysed by sonication on ice for 5 minutes in cycles of pulsing for 1 s on and 1 s off. Membranes were harvested from the cell lysate by ultracentrifugation at ~185,000xg for 1.5 hours. The membrane pellets were then resuspended in buffer (50 mM Tris-HCl, 300 mM NaCl, 30 mM Imidazole, pH 8.0, and protease inhibitors (Roche)) at a ratio of 16 mL of buffer per 1 g of membrane pellet. The membrane pellet was solubilized to homogeneity by dounce homogenization, then supplemented with iodoacetamide (1 mg/mL) and ß-dodecyl maltoside detergent (ß-DDM, 1% w/v) for detergent extraction of membrane proteins overnight at 4°C with stirring. The clarified supernatant containing solubilized protein was collected by ultracentrifugation at ~150,000xg for 30-40 minutes prior to purification.

Detergent-solubilized TmrAB was next purified by loading onto a Nickel affinity column (HisTrap IMAC HP, GE Healthcare) and washing with binding buffer (50 mM Tris-HCl, 300 mM NaCl, pH 8.0, 0.1% ß-DDM) containing increasing concentrations of Imidazole (Wash 1: 30 mM Imidazole (10CV), Wash 2: 100 mM Imidazole (3CV)). Protein was eluted in binding buffer containing 300 mM Imidazole (2CV) and immediately diluted into Imidazole-free buffer and concentrated for size exclusion chromatography (SEC). SEC purification was performed at 4°C on an Enrich SEC 650 column (Bio-Rad) and sample eluted in SEC buffer (20 mM HEPES, 150 mM NaCl, pH 7, and 0.05% ß-DDM). Peak fractions containing pure TmrAB (WT or mutant) were pooled, concentrated, and stored at -80°C prior to further experiments.

Negative stain analysis – Negatively-stained samples of WT and mutant TmrAB were prepared to evaluate the quality and architecture of purified sample (**Figure 2A**). Dilutions of purified TmrAB WT and mutant samples were prepared at 0.2 µM concentration in SEC buffer and 3 µL were applied to negative glow discharged carbon coated copper grids (EMS, Cat No. CF300-Cu-UL). Sample was incubated on grids for 30 s, then gently dipped in two drops of SEC buffer and one drop of 0.75% uranyl formate staining solution with blotting performed between drops by touching the grid edges to the surface of Whatman 1 filter paper. Grids were dipped in a second drop of stain for 30 s, blotted on filter paper, and air dried prior to imaging. Images were collected using a 120 kV Tecnai Spirit (FEI) microscope equipped with an AMT XR80L-B 8 x 8

CCD camera at 49,000X magnification corresponding to a pixel size of 2.21 Å.

Colorimetric ATPase assay – The specific ATP hydrolysis of TmrAB mutants was measured using two methods to evaluate ATPase activity at multiple temperatures. A colorimetric endpoint assay for inorganic phosphate determination described by Sarkadi et al. (23) was used to measure TmrAB ATPase activity near the physiological growth temperature of its host organism, *T. thermophilus* (68°C) (**Figure 2B**) and ambient temperature (25°C) (**Figure 3**). Purified samples of WT or mutant TmrAB (1 to 10 µg) in 40 µL assay buffer (50 mM MOPS-Tris pH 7.0, 50 mM KCl, and 2 µM DTT) were pre-incubated at 68°C for 5 minutes. The ATPase reaction was then started by the addition of 10 µL of Mg-ATP solution prepared in assay buffer, bringing the final concentration of TmrAB to 0.16 µM in a 50 µL reaction containing 10 mM $MgCl_2$ and varying final concentrations of ATP (0-6 mM). The concentration of TmrAB prepared for room temperature experiments was adjusted to 1.6 µM and rates calculated for a single concentration of ATP (8 mM). Samples in the absence of Mg-ATP solution or TmrAB were prepared as negative controls. The reaction was quenched for various time points by adding 40 µL 5% SDS. Following quenching, 200 µL of detection reagent (8.75 mM Ammonium Molybdate, 3.75 mM Zinc Acetate, pH 5.0, and 7.5% Ascorbic Acid pH 5.0) were added to each sample and incubated for 25 minutes at room temperature protected from light. The absorbance signal of total free phosphate in solution for each quenched sample and standards of KH_2PO_4 ranging in concentration from 0.0125 - 0.8 mM were subsequently measured at 800 nm in a clear 96-well plate (CoStar) on a BMG LabTech microplate reader. Michaelis-Menten curves are shown in **Figure 2B** as the mean ± standard deviation (S.D.) for data from three technical replicates (n=3) fit in Prism (GraphPad) with *Equation 1* below:

$$Y = \frac{(E_T * k_{cat}) * X}{(K_m + X)} \qquad \text{(Equation 1)}$$

Where Y is the enzyme velocity (mM/s), E_T is the total enzyme concentration (mM), k_{cat} is the turnover number (1/s), X is the concentration of ATP (mM), and K_m is the Michaelis-Menten constant (mM). Kinetic parameters (K_m, k_{cat}, V_{max}, and k_{cat}/K_m) are reported in **Table 1** as the mean ± standard error (S.E.).

Continuous enzyme-linked ATPase assay – ATPase activity for a subset of mutants alongside WT TmrAB was also measured using a continuous enzyme-coupled reaction system performed at room temperature as previously described (24). Samples were prepared as 75 µL reactions containing 5 µg of TmrAB (0.5 µM final concentration) in reaction buffer (20 mM HEPES pH 7.0, 10 mM $MgCl_2$, 5 mM ATP, 1 mM PEP, 0.45 mM NADH, 0.01% DDM, and Pyruvate Kinase (928U/mL)/Lactate Dehydrogenase (1300 U/mL) mix (Sigma)). The change in absorbance was monitored at 340 nm over 45 minutes at 15 second intervals in clear 96-well half-area plates (CoStar) on a Synergy Neo2 Multi-Mode Microplate Reader (Biotek). The relative enzyme velocities determined by linear regression are reported in **Supplemental Figure 3** as the percentage mean ± standard deviation (S.D.) normalized to the mean value for WT TmrAB for three replicates (n=3).

ATP binding assay – The binding affinity for nucleotide was measured as described in (11, 25) and the apparent K_D for a fluorescent analog of ATP, TNP-ATP (Molecular Probes), calculated for WT, G131A, G116A, and D117A TmrAB. Samples were prepared in a total volume of 50 µL containing 0.2 µM WT or mutant TmrAB in SEC buffer supplemented with 1 mM $MgCl_2$ and increasing concentrations of TNP-ATP (0-10 µM). Fluorescence data were immediately collected following the addition of TNP-ATP at 25°C in black 96-well half-area flat bottom microplates (CoStar) on a Synergy Neo2 Multi-Mode Microplate Reader (Biotek) at excitation and emission wavelengths of 408/10 nm and 535/15 nm, respectively. After subtracting for background fluorescence from TNP-ATP alone, data were normalized to the maximum fluorescence achieved within each dataset. Binding curves are shown in **Figure 4** as the mean ± S.D. for at least three technical replicates of WT, G116A and D117A TmrAB and two technical replicates for G131A TmrAB fit in Prism (GraphPad) with a one-site specific binding model using *Equation 2* below:

$$fb = \frac{B_{max} * [L]}{K_D + [L]} \qquad \text{(Equation 2)}$$

where *fb* is the fraction bound of protein with ligand, B_{max} is maximum binding, L is ligand, and K_D is the dissociation constant. Data for G131A TmrAB were subject to outlier analysis in Prism (GraphPad) prior to fitting. Apparent dissociation constants for TNP-ATP binding ($K_{D\text{-}app}^{TNP\text{-}ATP}$) are reported in **Table 2** as the mean ± S.E.

Peptide binding assay – The binding of fluorescent transport substrate peptide RRY($C^{Fluorescein}$)KSTEL (Genscript) was determined for WT, G131A, G116A, and D117A TmrAB as a function of the change in fluorescence polarization as described in (7, 14). In a total volume of 30 µL, 2 µM TmrAB in SEC buffer was incubated on ice for 15 minutes with 50 nM RRY($C^{Fluorescein}$)KSTEL and in the presence or absence of 5 mM ATP and 10 mM $MgCl_2$. Fluorescence polarization data were collected at 25°C in black 96-well half-area flat bottom microplates (CoStar) on a Synergy Neo2 Multi-Mode Microplate Reader (Biotek) at excitation and emission wavelengths of 485/20 nm and 520/20 nm, respectively. Data are reported in **Figure 5** as the percentage mean ± S.D. for three replicates (n=3) normalized to the mean value for WT TmrAB in the absence of ATP.

Results

The transmembrane domain (TMD) in ABC transporters is connected to the nucleotide binding domain (NBD) through helical extensions termed intracellular loops (ICL1 and ICL2) (**Figure 1A**). We investigated the highly conserved G(R/D)x_3Rx_3D motif of the peptide sensor in the TM3 cytoplasmic extension of ICL1. To test its role in allosteric coupling of ATP hydrolysis and substrate transport in TmrAB, we mutated conserved residues of the motif in both TmrA and TmrB chains (**Figure 1C**) and interrogated the effects on ATP hydrolysis (**Figure 2**), ATP binding (**Figure 3,4**), and substrate binding (**Figure 5**).

The peptide sensor motif in the transmembrane helix 3 extension is highly conserved in ABC transporters – We performed an analysis of nearly 500 sequences (202 related to TmrA, 250 related to TmrB) aligned in MUSCLE 3.8 (22) and defined a G(R/D)x_3Rx_3D consensus motif for the region in ICL1 connecting CH1 and TM3 identified as a peptide sensor in TAP1/TAP2 (**Figure 1C, Supplemental Figures 1, 2, 4**) (1, 2). This sequence is defined by 100% conservation of charged residues in the 1st, 6th, and 10th positions, with 100% conservation of the glycine in position 1 (G131 in TmrA, G116 in TmrB) and aspartate in position 10 (D140 in TmrA, D125 in TmrB). Every sequence contains a basic residue in position 6, with a high frequency of arginine (R136 in TmrA, R121 in TmrB). The charged residue in position 2 diverges between TmrA and TmrB, with strong conservation of a basic residue in TmrA (R132) and an acidic residue in TmrB (D117).

Mutations of conserved charged residues in the peptide sensor motif are structurally tolerated in Thermus thermophilus TmrAB – To test the function of charged residues in the peptide sensor motif, a total of 10 mutants of TmrAB were generated (G131A, R132A, R136A, and D140A in TmrA; G116A, D117A, R121A, and D125A in TmrB), expressed, and purified alongside wild-type (WT) TmrAB. Negative-stain electron microscopy analyses of mutant proteins purified into detergent-containing buffers confirmed the homogeneity of the mutants as well as the consistency of the architecture to known structures of TmrAB (**Figure 2A**). Mostly all of the mutants expressed and purified to similar yields as WT TrmAB using the expression protocol described, except for the G131A mutant which notably expressed to lower levels. The architecture of G131A TmrAB is nonetheless comparable to WT.

Mutation of conserved charged residues of the peptide sensor motif abrogates ATPase activity at physiological temperatures in TmrAB – TmrAB is derived from a thermophilic bacteria that exhibits optimal growth and function at 68°C (13), which is beyond the capabilities of most spectroscopic plate readers. To measure ATPase activity at 68°C we employed a colorimetric endpoint assay to evaluate the effect of mutating conserved charged residues of the sensor motif in TmrAB (R132A, R136A and D140A in TmrA; D117A, R121A, and D125A in TmrB) on ATP hydrolysis (**Figure 2B, Table 1**). At 68°C, WT TmrAB displayed characteristic ATPase activity with a measured K_m value of 1.269 ± 0.27 mM and a k_{cat} of 4.32 ± 0.318 ATP/s, consistent with previously published reports on WT TmrAB activity (7, 13). At this elevated temperature, all TmrA and TmrB charge mutants displayed significant decreases in ATPase activity, and a comparison of the initial

rates calculated for activity in the presence of 1 mM ATP revealed a ~5-10X reduction in activity compared to WT TmrAB (**Figure 2C**). The most significant effect was observed for the D117A mutation in TmrB. Mutation of its interaction partner in TmrB (R121A) as well as the homologous residue in TmrA (D140A) also resulted in a decrease in ATPase activity, but to a lesser extent.

Conserved glycines, G116 and G131, of the peptide sensor motif play distinct roles in conformational coupling – Both conserved glycines of the TmrAB peptide sensor motifs (G131 in TmrA, G116 in TmrB) are positioned at the base of the TM3 helical extension in a flexible turn after CH1 (**Figure 1B**). To identify their importance in the transition from inward to outward-facing states in TmrAB we mutated both to alanine (G131A in TmrA, G116A in TmrB) to restrict the intrinsic flexibility of the loop region while minimizing steric disruption of side chain packing. Analysis of ATPase activities of these mutants at 68°C demonstrated a loss of catalysis measured by the colorimetric ATPase assay, although to a lower extent (~4-5X reduction) than observed for mutants of the charged residues in the peptide sensor motif (**Figure 2B,C; Table 1**). While the rate of ATP turnover fell by approximately the same amount in both mutants relative to WT TmrAB, the K_m for ATP in G116A TmrAB (0.525 ± 0.133 mM) was half that of the G131A mutant (1.15 ± 0.251 mM) and WT TmrAB (1.29 ± 0.269 mM), corresponding to a catalytic efficiency (k_{cat}/K_m) of WT TmrAB that is ~4.2X and ~1.8X higher than of G116A or G131A TmrAB, respectively. While within the 95% confidence interval of the K_m values for both G131A and WT TmrAB, and unlikely to represent a significant change in this assay, it is potentially noteworthy that G131 in TmrA has slightly different effects on catalysis than G116 in TmrB.

To control for potential decreased stability in TmrAB mutants at higher temperatures, we performed a second assay for ATPase activity in WT, G131A, G116A, and D117A TmrAB at room temperature where TmrAB has minimal activity using both the ascorbic acid colorimetric assay (**Figure 3**) as well as a continuous enzyme-linked method (**Supplemental Figure 3**). As expected, the ATPase activity in WT TmrAB decreased to levels comparable to the activity of G116A and D117A TmrAB in both assays. Surprisingly, ATP hydrolysis at room temperature was significantly accelerated in G131A TmrAB, and a nearly 6-fold increase in activity relative to WT TmrAB was observed.

Mutation of the peptide sensor conserved glycine does not influence ATP binding –To rule out effects of mutation of the conserved glycines in the peptide sensor motif on nucleotide binding, and thus NBD dimerization, we determined the apparent affinity, $K_{D\text{-}app}^{TNP\text{-}ATP}$, for the fluorescent ATP analog, TNP-ATP, for both G131A and G116A TmrAB and as well as WT and D117A TmrAB included as controls (**Figure 4, Table 2**). The $K_{D\text{-}app}^{TNP\text{-}ATP}$ for each variant ranged from ~1.9 μM – 2.2 μM (**Table 2**). A Student's t-test resulted in P-values exceeding 0.05, which does not reject the null hypothesis, confirming no statistically significant difference in affinities for ATP between the mutants. This result suggests that the conformational flexibility of the peptide sensor helix is likely not a determinant for ATP binding, but instead may be critical for the transition to a conformational state optimal for ATP hydrolysis.

The G131A mutation interferes with the ability of TmrAB to achieve the low-affinity outward-facing conformation – To test the ability of the peptide sensor glycine mutants to adopt the low-affinity outward-facing conformation upon ATP binding, and thus substrate release, we employed a fluorescent polarization assay to monitor binding of a fluorescently-labeled peptide substrate (RRY($C^{Fluorescein}$)KSTEL) to WT, G131A, G116A, or D117A TmrAB in the presence and absence of ATP (**Figure 5**). In this assay, a polarization signal corresponds to peptide substrate binding (to a high-affinity site in the absence of ATP) in the inward-facing conformation of TmrAB. A decrease in the signal in the presence of saturating concentrations of ATP corresponds to a loss of peptide substrate, presumably through formation of the outward-facing state containing the low-affinity substrate binding site. Our results showed a statistically significant decrease in polarization in the presence of ATP for WT TmrAB and the G116A and D117A TmrB mutants of TmrAB, suggesting conformational coupling between the NBD and TMD proceeds as expected. However, the change in the polarization signal was not statistically significant for G131A TmrAB, indicating that the high-affinity state of the TmrA mutant may not switch to the low-affinity state in the presence of ATP in this mutant. These experiments were performed well below the

concentration where trans-inhibition of ATPase activity in over-stimulated ABC transporters is observed (26). This result highlights the importance of the conformational flexibility of ICL1 of TmrA, but not of TmrB, in the allosteric coupling of ATP hydrolysis and substrate release during the TmrAB transport cycle.

Discussion

The transport cycle of ABC transporters, vital for maintaining cellular homeostasis allosterically couples the chemical potential of cellular ATP to the thermodynamic work of directionally passing substrates over a membrane barrier. Complicated and still not entirely defined domain rearrangements of the allosteric mechanism help convert a high-affinity inward-facing state to a low-affinity outward-facing state.

Our results show how allosteric coupling for transition to the low-affinity outward-facing state depends on conserved residues of the peptide sensor G(R/D)x_3Rx_3D motif in intracellular loop 1 (ICL1). This motif forms a helix positioned in such a way that it could feasibly act as a conduit between the ATP-binding NBD and the TMD (**Figure 1A**). It is notable that a somewhat significant rotation and translation of ICL1 in TmrA appears to accompany a reorganization of its interaction network, but not to the same extent as in TmrB (**Figure 1B**) (27). This is consistent with our experimental results showing functional asymmetry in mutants of TmrAB designed to limit conformational change of the peptide sensor helix.

Surprisingly, the motif is conserved across all bacterial type-I ABC exporters even those that do not transport peptides such as the lipid A transporter MsbA and the multidrug transporters BmrCD and Sav1866 (**Supplemental Figures 1,2,4**). Furthermore, we found very high conservation of the first glycine residue in the motif (G131 in TmrA, G116 in TmrB) in every bacterial ABC1 family ABC exporter we were able to analyze (**Figure 1C; Supplemental Figures 1,2,4**). One notable exception, in *Thermotoga maritima* TM287/288 (16), one of the conserved glycines is substituted for a serine in the non-functional NBD. Conservation is also observed in nearly all human ABC exporters including P-glycoprotein (Pgp), TAP1/2, and MRP1. The only exception occurs in ABCD4, which nevertheless contains a hinge glycine directly before the coupling helix and after TM2 that may play a similar role as the peptide sensor glycine between CH1 and TM3 (28).

Based on recent cryo-EM structures, the conserved charged residues after the glycine align along one face of the peptide sensor helix. These amino acids rotate inward in the outward-facing conformation to make contacts with residues of CH1 and the TM4 ICL extension in TmrA or residues of TM4 and TM6 ICL extensions in TmrB, linking interactions with TMD helices and coupling helices adjacent to the NBD (**Figure 1B**) (7). Our catalytic results show that the ability to form these interactions and potentially conformationally couple ATP hydrolysis and substrate transport depends on the flexibility of the peptide sensor motif.

Several features of the motif support intrinsic flexibility. The first of these is a prominent π-helix in the C-terminus of the peptide sensor. Inherently flexible, π-helices are rare and found on average in only one of every six proteins (29). However, they are frequently observed in critical conformational junctions of dynamic integral membrane proteins, notably transporters and ion channels such as the bacterial amino acid transporter LeuT (29, 30), the human temperature sensitive channels of the TRPV family (31–35), and in the outward-facing states of ABC transporters (7, 19, 20). In these proteins, the π-helix has been suggested to permit a peristaltic like motion between the helix and its environment, enabling multiple interactions to form and break within a tightly packed helical bundle (29). In the TRPV family, a π-helix forms a conformational switch from open to closed, and a similar α-helix to 3_{10} helix switch was also described as important for gating in the Potassium (36) and HCN channels (37). In this context, the inhibitory effect of our mutations in the TmrAB peptide sensor π-helices may be due to the loss of ICL1 conformations necessary for TmrAB to proceed through its catalytic cycle, or may simply be due to the loss of the electrostatic interactions facilitated by charged residues of the π-helix.

A second potentially important determinant of peptide sensor flexibility is the glycine found at the base of the motif helix in TmrA (G131) and TmrB (G116) and forms a critical hinge. Glycine in general confers flexibility to protein loops and turns, and mutation to alanine restricts the protein backbone with the least steric interference. We observed completely different effects of this mutation on catalysis and conformational coupling in each half of

TmrAB. Mutation in TmrB (G116A) inhibited ATP hydrolysis, but not conformational coupling, whereas mutation in TmrA (G131A) unexpectedly elevated ATPase activity while also eliminating the ability of TmrAB to transition to a low-affinity peptide binding state (consistent with either the outward facing or outward occluded cryo-EM structures (7)) (**Figure 6A**). The latter outcome mimics the effect seen in Pgp for mutations of the flexible Q-loop decoupling ATPase activity from the transport cycle (38). From this perspective, we rationalize that G116A TmrB can attain an outward-facing conformation, albeit at a slower rate (**Figure 6B**). Limiting the TmrB peptide sensor helix mobility likely results in a slower overall transport cycle in TmrB that nevertheless is still conformationally intact.

In opposition to our TmrB results, our data suggests G131A TmrA disrupts formation of the low-affinity outward-facing conformation central to the alternating access model (**Figure 6B**) (4). Supporting evidence comes from studies in TAP1/2 in which mutation of one of these glycines to a cysteine decreased transport ~4-fold and crosslinks in this region between the NBD and the ICL1 loop interfered with transport (2). Altogether, these results underscore a direct relationship between this hinge region and the transport cycle. Specifically, our data suggest that the outward-facing transition in TmrAB is reinforced by the formation of an electrostatic network of interactions that 1) directly couple the NBD in its nucleotide-bound state and the TMD and 2) stabilize the outward-facing conformation of TmrAB in its low-affinity state.

In summary, our results indicate that the stability of the outward-facing state (or outward occluded) may not only depends on a network of electrostatic interactions extending from the peptide sensor motif, but that the transition to the low-affinity for substrate, outward-facing state may also rely on the conformational flexibility of TmrA ICL1 peptide sensor in this half of TmrAB. These results are consistent with the switch model, as well as recent modifications that incorporate ATP hydrolysis either as the driver of inward to outward facing conformations (6) or substrate release (7). Our results are also consistent with the formation of intermediates such as the outward-occluded state (7) in which similar sets of interactions as shown in **Figure 1B** are observed. We however cannot fully explain why uncoupling of ATP binding and hydrolysis from formation of the low-affinity substrate binding state is observed for only one (G131A TmrA) of the two conserved glycine mutants.

Several non-mutually exclusive hypotheses are consistent with our findings. First, a higher ATPase rate might result from NBD uncoupling from the TMD when conformational feedback from the peptide binding region is lost and the protein is trapped in the high-affinity state (as in the case of the G131A TmrA mutant). Alternatively, the conformational states that promote efficient catalysis may be driven by one half of the protein, and the state that promotes substrate release is driven by the other half. Together, tight regulation is imposed on the activities in the other half, and the loss of global regulation could potentially accelerate the ATPase rate. In this scenario, the peptide sensor helix is an important regulatory switch along a different part of the transport cycle in each half of TmrAB, instead of as a general mechanical couple, and conformational changes in the NBD are imparted to the TMD globally instead of through a few local interactions. Additional detailed kinetics, time-resolved structural biology, and large-scale molecular dynamics will likely be required to establish the appropriate model.

ACKNOWLEDGEMENTS

This was work was supported by grants from the National Institute of General Medicine Sciences to T.M.T (R00 GM11424). We thank Nitesh Khandelwal in the Tomasiak lab for helpful discussions.

DECLARATION OF INTEREST

The authors declare no competing interests.

Table 1. ATPase activity of TrmAB and Peptide Sensor mutants

Protein	K_m [mM][a]	k_{cat} [s^{-1}][b]	V_{max} (mM/s)[c]	k_{cat}/K_m [$s^{-1}mM^{-1}$]
WT	1.29 ± 0.269	4.32 ± 0.318	6.92 x10^4	3.36
G131A	1.15 ± 0.251	1.09 ± 0.0811	1.74 x10^4	0.951
R132A	1.08 ± 0.194	1.84 ± 0.111	2.95 x10^4	1.71
R136A	1.16 ± 0.443	0.732 ± 0.0952	1.17 x10^4	0.632
D140A	0.587 ± 0.250	0.832 ± 0.0999	1.33 x10^4	1.42
G116A	0.525 ± 0.133	0.951 ± 0.0660	1.52 x10^4	1.81
D117A	0.660 ± 0.223	0.463 ± 0.0475	7.40 x10^4	0.749
R121A	0.755 ± 0.183	0.706 ± 0.0515	1.13 x10^4	0.936
D125A	1.20 ± 0.318	0.766 ± 0.0697	1.22 x10^4	0.637

[a,b] K_m and k_{cat} values were obtained from data presented in **Figure 2** fitted by nonlinear regression analysis using Equation 1 in Prism (GraphPad).
[c] V_{max} was calculated as $E_T * k_{cat}$, where E_T is the total enzyme concentration in the assay (0.16 μM). Data reported are the mean ± standard error (S.E.) for data collected in triplicate.

Table 2. Apparent nucleotide binding affinities for TmrAB and Peptide Sensor mutants

Protein	$K_{D\text{-}app}^{TNP}$ [μM][d]	P-value[e]
WT	2.18 ± 1.12	---
G131A	4.00 ± 0.913	0.3448
G116A	4.55 ± 1.21	0.1756
D117A	1.86 ± 0.391	0.7404

[d] $K_{D\text{-}app}^{TNP\text{-}ATP}$ values were obtained from data presented in **Figure 4** fitted by nonlinear regression analysis using Equation 2 in Prism (GraphPad). Data reported are the mean ± S.E.
[e] P-value denotes probability of the null-hypothesis that the mutant mean is equal to that of WT TmrAB.

FIGURES

Figure 1

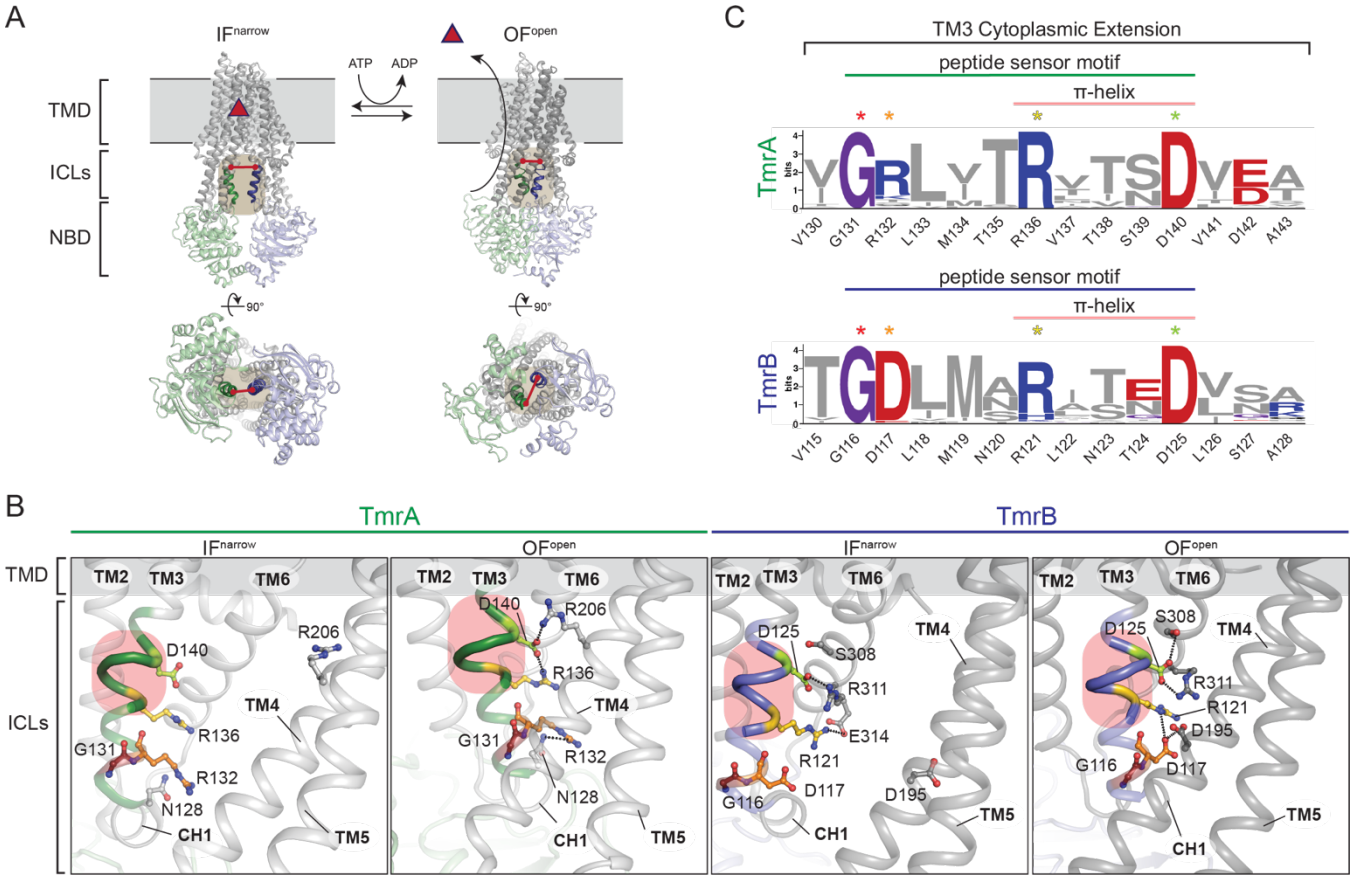

Figure 1. Overview of the Peptide Sensor Motif in Intracellular Loop 1 (ILC-1) of TmrAB. A) Cartoon overview of inward-facing (PDBID: 6RAF (7)) to outward-facing (PDBID: 6RAJ (7)) transitions of TmrAB highlighting relative orientations of the transmembrane domain (TMD), intracellular loops (ICLs), and nucleotide binding domains (NBD) from TmrA (*light grey* TMD and ICLs with *light green* NBD) and TmrB (*dark grey* TMD and ICLs with *light blue* NBD) at the proposed start and end of the putative transport cycle. The regions corresponding to the peptide sensor helix region in the transmembrane 3 (TM3) cytoplasmic extension of intracellular loop 1 (ICL1) are shown in *green* for chain A (TmrA) and in *blue* for chain B (TmrB). The red line represents the relative distances in peptide sensor helices in each state. **B)** Cartoon and stick representation highlighting local rearrangements in the interaction network of the peptide sensor helix in TmrA (*green* ribbon, left panels) and TmrB, *blue* ribbon, right panels) in proximity of coupling helix 1 (CH1) and transmembrane helices (TM2-6) in the inward-facing (PDBID: 6RAF (7), left panels) and outward-facing (PDBID: 6RAJ (7), right panels) states. Interactions between residue pairs are shown as dashed lines. Equivalent residues of the peptide sensor helix in TmrA and TmrB are colored the same (G131/G116 in red, R132/D117 in orange, R1121 in yellow, D140/D125 in green). A segment of the peptide sensor forming a π-helix is highlighted in *pink*. **C)** WebLogo diagram illustrating sequence conservation in alignments of the ICL1 TM3 cytoplasmic extension in TmrA (202 sequences) and TmrB (250 sequences), highlighting the consensus sequence of the peptide sensor motif and the corresponding residues forming the observed π-helix shown in (***B***). Numbering below each Logo corresponds to the sequence in TmrA or TmrB, and asterisks (*) denote positions mutated in this study.

Figure 2

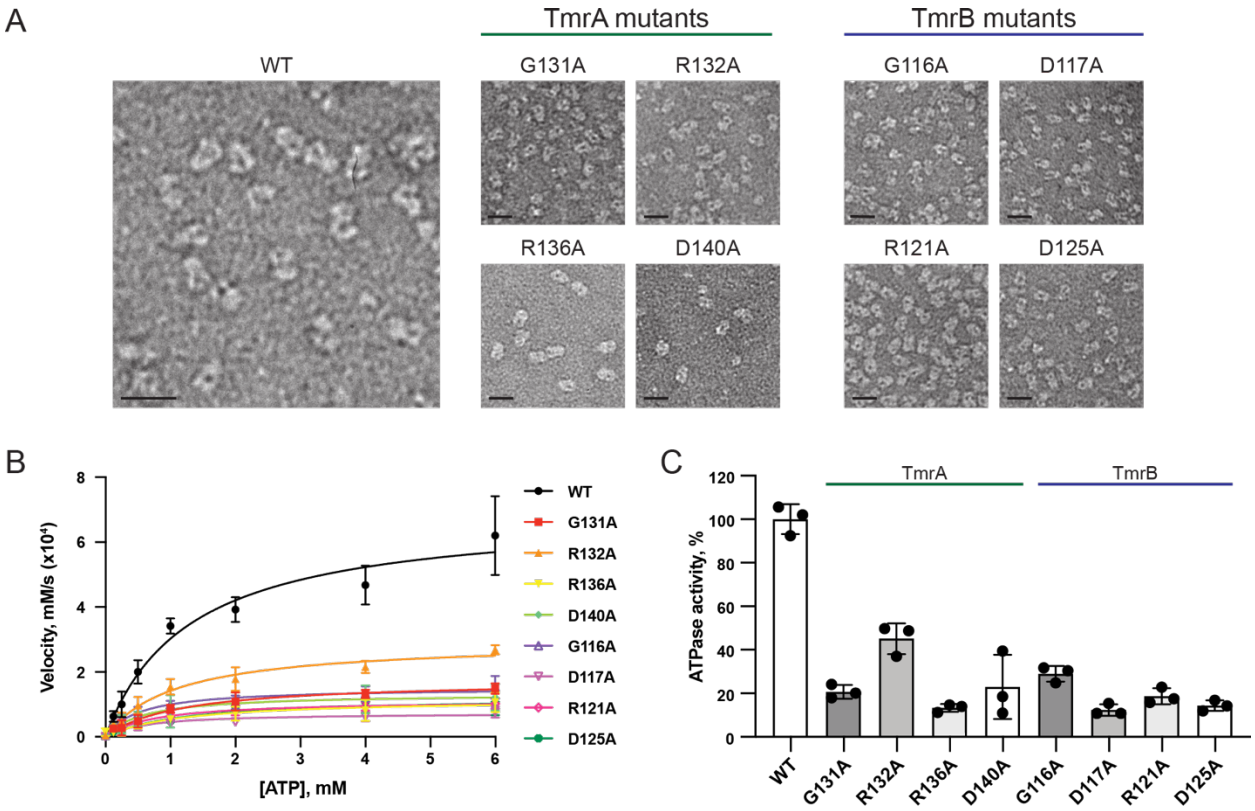

Figure 2. Mutations in the Peptide Sensor Motif of ICL1 disrupt ATPase activity in TmrAB at physiological temperatures. A) Negative-stain images of purified wild-type (WT) and mutant TmrAB collected at 49,000X magnification. Scale bars correspond to 20 nm. **B)** ATP hydrolysis activity at 68°C measured using the ascorbic acid colorimetric assay (described in Experimental Methods) for 0.16 µM WT or mutant variants of TmrAB shown in (***A***) and varying concentrations of ATP. Michaelis-Menten kinetic parameters K_m, k_{cat}, and k_{cat}/K_m were determined using Prism (GraphPad) and are summarized in **Table 1**. **C)** The ATPase activities determined for WT and mutant TmrAB in the presence of 1 mM ATP reported in (***B***) normalized to the mean value for WT TmrAB to demonstrate the inhibitory effect of peptide sensor motif mutation on ATP hydrolysis at 68°C. Data in (***B***) and (***C***) are the mean ± standard deviation (S.D.) for three replicates (n =3).

Figure 3

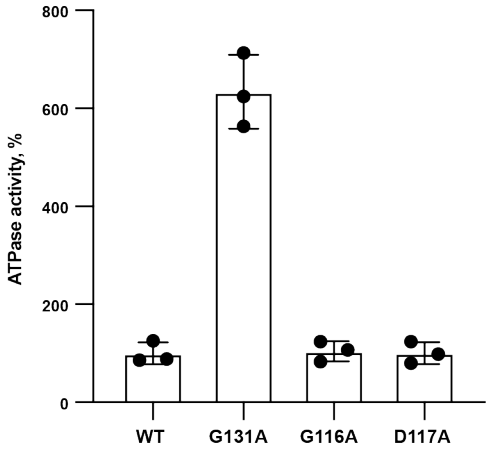

Figure 3. G131A accelerates ATP hydrolysis in TmrAB at room temperature. ATPase activity at room temperature determined for variants of TmrAB mutated at the absolutely conserved glycine residues of the peptide sensor motif (G131A in TmrA and G116A in TrmB) compared to WT and the TmrB D117A mutant shown in Figure 2 to be the least active as a control. ATPase data were collected for 1.6 μM enzyme in the presence of 8 mM ATP using the ascorbic acid colorimetric assay described in Experimental Methods, and reported here as the normalized mean ± S.D. for three replicates (n =3).

Figure 4

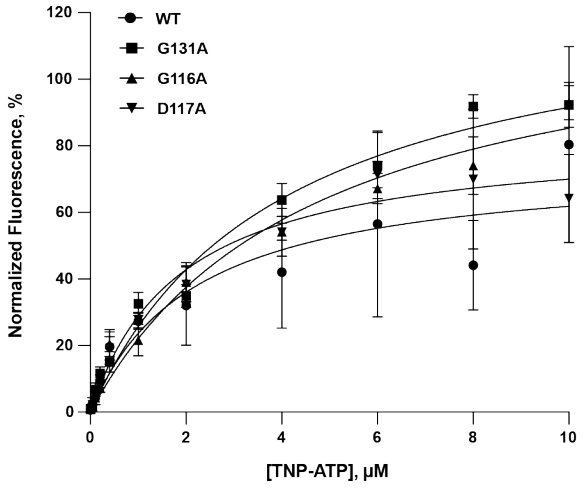

Figure 4. Mutant TmrAB exhibits ATP affinities similar to wild-type TmrAB. The change in fluorescence at room temperature for WT or mutant TmrAB (0.2 μM) in the presence of increasing concentrations of the fluorescent ATP analog, TNP-ATP (Sigma). Data are presented as the percentage mean ± S.D. for at least three replicates (n=3). Apparent binding affinities for TNP-ATP ($K_{D\text{-}app}^{TNP\text{-}ATP}$) were determined using Prism (GraphPad) and are summarized in **Table 2**.

Figure 5

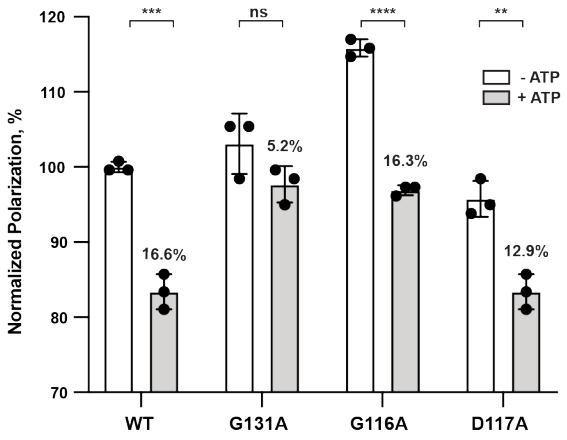

Figure 5. Peptide sensor mutation G131A uncouples substrate binding from NBD dimerization. The change in fluorescence polarization was monitored for WT and mutant TmrAB (2 μM) incubated with 50 nM of the fluorescent transport substrate peptide, RRY($C^{Fluorescein}$)KSTEL and in the presence (*white* bars) or absence (*grey* bars) of 5 mM ATP added to achieve the outward-facing state. Data are presented as the percentage mean ± S.D. for three replicates (n=3) normalized to the mean value for WT TmrAB in the absence of ATP. P-values are reported above the data (ns: not significant ($P \geq 0.05$), **: $P \leq 0.01$, ***: $P \leq 0.001$, ****: $P \leq 0.0001$).

Figure 6

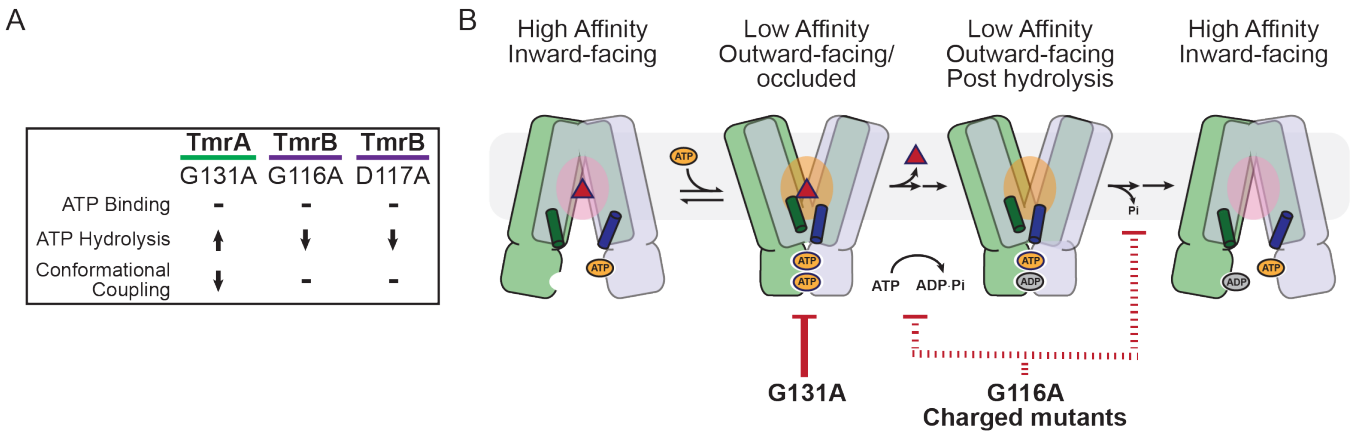

Figure 6. Schematic overview of peptide sensor mutant effects on the transport cycle of TmrAB. A) Summary of the observed change in TmrAB transporter functions for peptide sensor mutants. Arrows indicate increase or decrease. Dash indicates no change. **B)** Simplified overview of a TmrAB transport cycle based on previously reported structural intermediates (7) and the proposed states disrupted by peptide sensor mutants described here. TmrA and TmrB are colored *light green* and *light purple*, respectively. The peptide sensor helices of each chain are shown as cartoon helices (*dark green* in TmrA; *dark blue* in TmrB). The high affinity substrate binding site is shown as an oval that is colored *light pink*, whereas the low affinity site is shown as an oval that is colored *light orange*. The *red* triangle represents substrate, ATP is an orange oval, and ADP is a grey oval.

Supplemental Figure 1

See attached alignment file.

Supplemental Figure 1. Sequence alignments of homologous sequences of TmrA. A total of 202 homologous sequences of TmrA were selected and downloaded from UniProt. Alignments were performed in MUSCLE 3.8 (22).

Supplemental Figure 2

See attached alignment file.

Supplemental Figure 2. Sequence alignments of homologous sequences of TmrB. A total of 250 homologous sequences of TmrB were selected and downloaded from UniProt. Alignments were performed in MUSCLE 3.8 (22).

Supplemental Figure 3

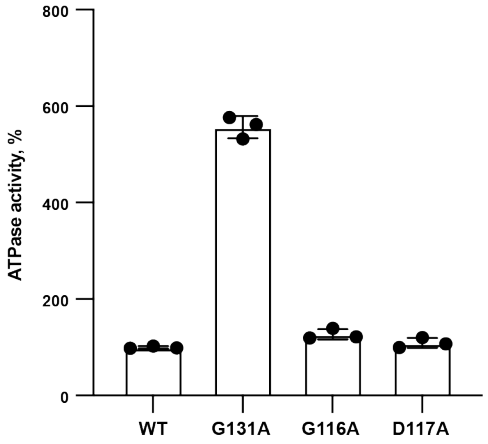

Supplemental Figure 3. ATPase activity for variants of TmrAB and WT at room temperature determined by enzyme-coupled assay. ATPase data collected for mutants of the absolutely conserved glycine residues of the peptide sensor motif (G131A in TmrA and G116A in TrmB) compared to WT and the D117A TmrB mutant. Data were collected for 0.5 μM enzyme in the presence of 5 mM ATP. Data are reported here as the normalized mean ± S.D. for three replicates (n =3).

Supplemental Figure 4

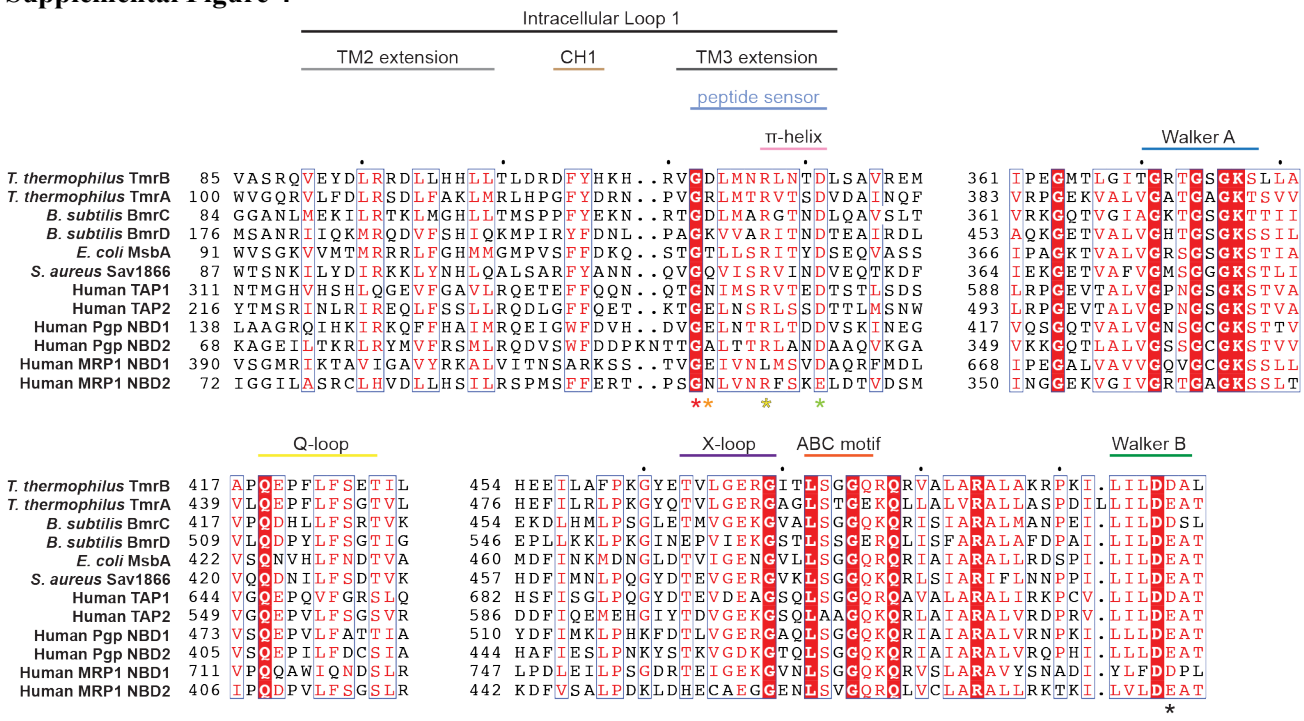

Supplemental Figure 4. Sequence alignment of conserved functional elements in representative members of ABC transporter families. Sequences were aligned in ClustalW (39) and colored in ESPript 3.0 (40) by similarity. Residues of the peptide sensor mutated in this study are denoted by an asterisk colored the same as for **Figure 1** in the main text. The catalytic glutamate (E) in the Walker B motif is highlighted with a black asterisk below the sequence. Sequences containing an aspartate (D) in this position are considered non-functional for ATP hydrolysis.

REFERENCES

1. Herget, M., Oancea, G., Schrodt, S., Karas, M., Tampe, R., and Abele, R. (2007) Mechanism of substrate sensing and signal transmission within an ABC transporter: Use of a Trojan horse strategy. *J. Biol. Chem.* **282**, 3871–3880
2. Oancea, G., O'Mara, M. L., Bennett, W. F. D., Tieleman, D. P., Abele, R., and Tampé, R. (2009) Structural arrangement of the transmission interface in the antigen ABC transport complex TAP. *Proc. Natl. Acad. Sci. U. S. A.* **106**, 5551–5556
3. Holland, I. B. (2019) Rise and rise of the ABC transporter families. *Res. Microbiol.* **170**, 304-320
4. Jardetzky, O. (1966) Simple allosteric model for membrane pumps. *Nature*. **211**, 969–970
5. Higgins, C. F., and Linton, K. J. (2004) The ATP switch model for ABC transporters. *Nat. Struct. Mol. Biol.* **11**, 918–926
6. Verhalen, B., Dastvan, R., Thangapandian, S., Peskova, Y., Koteiche, H. A., Nakamoto, R. K., Tajkhorshid, E., and McHaourab, H. S. (2017) Energy transduction and alternating access of the mammalian ABC transporter P-glycoprotein. *Nature*. **543**, 738–741
7. Hofmann, S., Januliene, D., Mehdipour, A. R., Thomas, C., Stefan, E., Brüchert, S., Kuhn, B. T., Geertsma, E. R., Hummer, G., Tampé, R., and Moeller, A. (2019) Conformation space of a heterodimeric ABC exporter under turnover conditions. *Nature*. **571**, 580–583
8. Dalmas, O., Orelle, C., Foucher, A. E., Geourjon, C., Crouzy, S., Di Pietro, A., and Jault, J. M. (2005) The Q-loop disengages from the first intracellular loop during the catalytic cycle of the multidrug ABC transporter BmrA. *J. Biol. Chem.* **280**, 36857–36864
9. Urbatsch, I. L., Gimi, K., Wilke-Mounts, S., and Senior, A. E. (2000) Investigation of the role of glutamine-471 and glutamine-1114 in the two catalytic sites of P-glycoprotein. *Biochemistry*. **39**, 11921–11927
10. Doshi, R., and van Veen, H. W. (2013) Substrate binding stabilizes a pre-translocation intermediate in the ATP-binding cassette transport protein MsbA. *J. Biol. Chem.* **288**, 21638–21647
11. Doshi, R., Ali, A., Shi, W., Freeman, E. V, Fagg, L. A., and van Veen, H. W. (2013) Molecular disruption of the power stroke in the ATP-binding cassette transport protein MsbA. *J. Biol. Chem.* **288**, 6801–6813
12. Bechara, C., Nöll, A., Morgner, N., Degiacomi, M. T., Tampé, R., and Robinson, C. V. (2015) A subset of annular lipids is linked to the flippase activity of an ABC transporter. *Nat. Chem.* **7**, 255–262
13. Zutz, A., Hoffmann, J., Hellmich, U. A., Glaubitz, C., Ludwig, B., Brutschy, B., and Tampé, R. (2011) Asymmetric ATP Hydrolysis Cycle of the Heterodimeric Multidrug ABC Transport Complex TmrAB from *Thermus thermophilus*. *J. Biol. Chem.* **286**, 7104–7115
14. Nöll, A., Thomas, C., Herbring, V., Zollmann, T., Barth, K., Mehdipour, A. R., Tomasiak, T. M., Brüchert, S., Joseph, B., Abele, R., Oliéric, V., Wang, M., Diederichs, K., Hummer, G., Stroud, R. M., Pos, K. M., and Tampé, R. (2017) Crystal structure and mechanistic basis of a functional homolog of the antigen transporter TAP. *Proc. Natl. Acad. Sci. U. S. A.* **114**, E438–E447
15. Grossmann, N., Vakkasoglu, A. S., Hulpke, S., Abele, R., Gaudet, R., and Tampé, R. (2014) Mechanistic determinants of the directionality and energetics of active export by a heterodimeric ABC transporter. *Nat. Commun.* **5**, 5419
16. Hohl, M., Briand, C., Grütter, M. G., and Seeger, M. A. (2012) Crystal structure of a heterodimeric ABC transporter in its inward-facing conformation. *Nat. Struct. Mol. Biol.* **19**, 395–402
17. Kim, J. M., Wu, S., Tomasiak, T. M., Mergel, C., Winter, M. B., Stiller, S. B., Robles-Colmanares, Y., Stroud, R. M., Tampé, R., Craik, C. S., and Cheng, Y. (2015) Subnanometre-resolution electron cryomicroscopy structure of a heterodimeric ABC exporter. *Nature*. **517** 396-400
18. Oldham, M. L., Hite, R. K., Steffen, A. M., Damko, E., Li, Z., Walz, T., and Chen, J. (2016) A mechanism of viral immune evasion revealed by cryo-EM analysis of the TAP transporter. *Nature*. **529**, 537–540
19. Ward, A., Reyes, C. L., Yu, J., Roth, C. B., and Chang, G. (2007) Flexibility in the ABC transporter MsbA: Alternating access with a twist. *Proc. Natl. Acad. Sci. U. S. A.* **104**, 19005–19010
20. Dawson, R. J. P., and Locher, K. P. (2006) Structure of a bacterial multidrug ABC transporter. *Nature.* **443**, 180–185

21. Liu, H., and Naismith, J. H. (2008) An efficient one-step site-directed deletion, insertion, single and multiple-site plasmid mutagenesis protocol. (2008) *BMC Biotechnol.* **8**, 91
22. Edgar, R. C. (2004) MUSCLE: multiple sequence alignment with high accuracy and high throughput. *Nucleic Acids Res.* **32**, 1792–1797
23. Sarkadi, B., Pricet, E. M., Boucherg, R. C., Germannil, U. A., and Scarboroughv, G. A. (1992) Expression of the Human Multidrug Resistance cDNA in Insect Cells Generates a High Activity Drug-stimulated Membrane ATPase. *J. Biol. Chem.* **267**, 4854-4858
24. Sehgal, P., Olesen, C., and Møller, J. V. (2016) ATPase activity measurements by an enzyme-coupled spectrophotometric assay. *Methods Mol. Biol.* **1377**, 105–109
25. Stewart, R. C., Vanbruggen, R., Ellefson, D. D., and Wolfe, A. J. (1998) TNP-ATP and TNP-ADP as Probes of the Nucleotide Binding Site of CheA, the Histidine Protein Kinase in the Chemotaxis Signal Transduction Pathway of Escherichia coli. (1998) *Biochemistry.* **37**, 12269-12279
26. Barth, K., Hank, S., Spindler, P. E., Prisner, T. F., Tampé, R., and Joseph, B. (2018) Conformational Coupling and trans-Inhibition in the Human Antigen Transporter Ortholog TmrAB Resolved with Dipolar EPR Spectroscopy. *J. Am. Chem. Soc.* **140**, 4527–4533
27. Hofmann, S., Januliene, D., Mehdipour, A. R., Thomas, C., Stefan, E., Brüchert, S., Kuhn, B. T., Geertsma, E. R., Hummer, G., Tampé, R., and Moeller, A. (2019) Conformation space of a heterodimeric ABC exporter under turnover conditions. *Nature*. **571**, 580–583
28. Xu, D., Feng, Z., Hou, W. T., Jiang, Y. L., Wang, L., Sun, L., Zhou, C. Z., and Chen, Y. (2019) Cryo-EM structure of human lysosomal cobalamin exporter ABCD4. (2019) *Cell Res.* **29**, 1039-1041
29. Cooley, R. B., Arp, D. J., and Karplus, P. A. (2010) Evolutionary Origin of a Secondary Structure: α-Helices as Cryptic but Widespread Insertional Variations of α-Helices That Enhance Protein Functionality. *J. Mol. Biol.* **404**, 232–246
30. Yamashita, A., Singh, S. K., Kawate, T., Jin, Y., and Gouaux, E. (2005) Crystal structure of a bacterial homologue of Na+/Cl --dependent neurotransmitter transporters. *Nature*. **437**, 215–223
31. Zubcevic, L., Herzik, M. A., Wu, M., Borschel, W. F., Hirschi, M., Song, A. S., Lander, G. C., and Lee, S. Y. (2018) Conformational ensemble of the human TRPV3 ion channel. *Nat. Commun.* **9**, 4773
32. Cao, E., Liao, M., Cheng, Y., and Julius, D. (2013) TRPV1 structures in distinct conformations reveal activation mechanisms. *Nature*. **504**, 113–118
33. McGoldrick, L. L., Singh, A. K., Saotome, K., Yelshanskaya, M. V., Twomey, E. C., Grassucci, R. A., and Sobolevsky, A. I. (2018) Opening of the human epithelial calcium channel TRPV6. *Nature.* **553**, 233–237
34. Zhang, F., Swartz, K. J., and Jara-Oseguera, A. (2019) Conserved allosteric pathways for activation of TRPV3 revealed through engineering vanilloid-sensitivity. *Elife*. 10.7554/eLife.42756
35. Singh, A. K., McGoldrick, L. L., and Sobolevsky, A. I. (2018) Structure and gating mechanism of the transient receptor potential channel TRPV3. *Nat. Struct. Mol. Biol.* **25**, 805–813
36. Long, S. B., Tao, X., Campbell, E. B., and MacKinnon, R. (2007) Atomic structure of a voltage-dependent K+ channel in a lipid membrane-like environment. *Nature*. **450**, 376–382
37. Lee, C., and MacKinnon, R. (2019) Voltage Sensor Movements during Hyperpolarization in the HCN Channel. (2019) *Cell*. **179**, 1582-1589
38. Zolnerciks, J. K., Akkaya, B. G., Snippe, M., Chiba, P., Seelig, A., and Linton, K. J. (2014) The Q loops of the human multidrug resistance transporter ABCB1 are necessary to couple drug binding to the ATP catalytic cycle. *FASEB J. Res. Commun.* **10**, 4335-4346
39. Sievers, F., Wilm, A., Dineen, D., Gibson, T. J., Karplus, K., Li, W., Lopez, R., McWilliam, H., Remmert, M., Söding, J., Thompson, J. D., and Higgins, D. G. (2011) Fast, scalable generation of high-quality protein multiple sequence alignments using Clustal Omega. *Mol. Syst. Biol.* **7**, 539
40. Robert, X., and Gouet, P. (2014) Deciphering key features in protein structures with the new ENDscript server. *Nucleic Acids Res.* **42**, W320–W324